6-2022

Poly (5-Carboxyindole)–β-Cyclodextrin Composite Material for Enhanced Formaldehyde Gas Sensing

John N. Hodul
Purdue University

Nikhil F. Carneiro
Purdue University

Allison K. Murray
Marquette University, allison.murray@marquette.edu

Wilson Lee
Purdue University

Kelly M. Brayton
Purdue University

See next page for additional authors

Journal of Materials Science, Vol. 57, No. 24 (june 2022): 11460-11474. DOI.

Poly (5-carboxyindole)–β-cyclodextrin Composite Material for Enhanced Formaldehyde Gas Sensing

John N. Hodul
Department of Chemistry, Purdue University, West Lafayette, IN
Nikhil F. Carneiro
School of Mechanical Engineering, Purdue University, West Lafayette, IN
Ray W. Herrick Laboratories, Purdue University, West Lafayette, IN
Allison K. Murray
School of Mechanical Engineering, Purdue University, West Lafayette, IN
Ray W. Herrick Laboratories, Purdue University, West Lafayette, IN
Wilson Lee
Charles D. Davidson School of Chemical Engineering, Purdue University, West Lafayette, IN
Kelly M. Brayton
Department of Chemistry, Purdue University, West Lafayette, IN
Xinping He
Charles D. Davidson School of Chemical Engineering, Purdue University, West Lafayette, IN
Carsten Flores-Hansen

Department of Chemistry, Purdue University, West Lafayette, IN
Dmitry Zemlyanov
Birck Nanotechnology Center, Purdue University, West Lafayette, IN
George T.-C. Chiu
School of Mechanical Engineering, Purdue University, West Lafayette, IN
Ray W. Herrick Laboratories, Purdue University, West Lafayette, IN
James E. Braun
School of Mechanical Engineering, Purdue University, West Lafayette, IN
Ray W. Herrick Laboratories, Purdue University, West Lafayette, IN
Bryan W. Bourdouris
Department of Chemistry, Purdue University, West Lafayette, IN
Charles D. Davidson School of Chemical Engineering, Purdue University, West Lafayette, IN
Jeffrey F. Rhoads
School of Mechanical Engineering, Purdue University, West Lafayette, IN
Ray W. Herrick Laboratories, Purdue University, West Lafayette, IN
Birck Nanotechnology Center, Purdue University, West Lafayette, IN

Abstract

Formaldehyde, a compound commonly employed in many construction materials, paints, and plastics, has been linked to deleterious health effects. Thus, monitoring the presence of formaldehyde in interior locations is increasingly important when it comes to public health. Currently, there is a crucial need for a low-cost, small-scale, selective, and sensitive indoor sensor capable of real-time formaldehyde detection. To meet these performance metrics, materials need to be incorporated onto existing gas sensor platforms to act as chemically selective recognition layers. A main challenge when addressing this issue is creating a material that can remain easily processable, can be easily synthesized, and can operate in practical environments (i.e., at common temperatures, humidity values, and in the presence of distractant analytes). Here, we show the unique properties of poly(5-carboxyindole) (P5C), an easily synthesized polymer, for practical indoor air monitoring of formaldehyde gas at concentrations as low as 25 ppm with rapid response and recovery times characterized by time constants of 27 s and 16 s, respectively. Importantly, we demonstrate that β-cyclodextrin (BCD), when blended into P5C to create a poly(5-carboxyindole) with β-cyclodextrin composite (P5C–BCD), offers distinct properties that enhance the response to formaldehyde gas in common operational conditions. Specifically, BCD adds features into the P5C such as its ability to form strong host–guest interactions with formaldehyde, its ability to buffer P5C protonation states to allow for more protonated carboxylic acid moieties on P5C which can hydrogen bond more effectively with formaldehyde, as well as creating a cylindrical morphology with the polymer film to assist the diffusion of formaldehyde into the polymer matrix. Additionally, these materials provide for chemically selective adsorption to formaldehyde gas in environments where interfering analytes exist. Due to the practical advantages these materials offer, they have the potential to unlock new avenues for future formaldehyde sensor materials.

Introduction

Volatile organic compounds (VOCs) are widely found in the manufacturing of indoor household materials [1]. These materials include structural building elements, carpeting, wood, adhesives, coatings, paints, and plastic products [2-5]. However, many of these indoor household materials can emit VOCs over time, thus affecting the quality of indoor air. Indoor air quality can be a major health concern due to the many health risk factors that have been associated with VOCs [6]. For instance, formaldehyde is a VOC that is primarily released from the aforementioned materials over time [8], and exposure to formaldehyde can cause irritation of the eyes, skin, and the respiratory and nervous systems in the short term [9-12]. Additionally, long-term exposure to formaldehyde has been linked to acute myeloid leukemia and Hodgkin's disease [13-16]. Thus, the World Health Organization (WHO) has set a 30 min exposure limit of 0.08 ppm for formaldehyde, while the US National Institute for Occupational Safety and Health (NIOSH) has established a maximum long-term exposure limit (TWA) of 0.016 ppm for formaldehyde [17]. Due to these low exposure limits, there is a compelling need for an energy-efficient, low-cost, and reliable sensing platform that is designed to detect formaldehyde with high sensitivity that also is small in area and lightweight such that it can be used easily in interior spaces.

Various types of sensor platforms have been utilized for monitoring formaldehyde gas. These techniques include spectrophotometry, gas chromatography, high-performance liquid chromatography, ion chromatography, polarography, fluorescence spectroscopy, and ultraviolet–visible (UV–Vis) light spectroscopy [19-23]. These approaches, though effective at detecting formaldehyde, are not realistic to implement in common indoor air quality monitoring end-use cases due to their bulky instrumentation, and they are largely unable to detect formaldehyde in a real-time manner. This has created a market for lower-cost and smaller-scale sensors that operate mainly through electrochemical or electromechanical mechanisms that use a selective chemical recognition layer [1], [24-29]. These sensors have shown great success with respect to their small sizes, their ability to be portable, and their detection of formaldehyde gas (i.e., as low as 1 ppm) [30-34]. However, electrochemical-based sensors are limited by their surface chemistry, which typically requires metal or graphene additives to provide a conductive media to measure conductivity changes on the device. This can make fabrication difficult and create selectivity issues when trying to detect the target analyte in the presence of interfering gases [35]. One sub-category of electrochemical sensors, metal oxide sensors, utilize electron donors or electron acceptors in the gas phase, which can adsorb onto a metal oxide-based material. In most cases, this adsorption requires high temperatures (i.e., >150 °C) or UV light during operation, which allows the adsorbed species to exchange electrons with the metal oxide. Unfortunately, this heating and photochemical processes require high energy input [3], [36-38]. There are metal oxide sensors that operate at room temperature, but these require additives and/or extensive processing techniques to acquire a reliable response [38-40]. Electromechanical sensors, such as gravimetric sensors, offer the advantage of not requiring the sensing material to be conductive, which broadens the range of useable sensing materials. These sensors have shown much promise in the area of formaldehyde detection, detecting formaldehyde in the ppb concentration range [41-43]. However, these materials suffer from many of the same disadvantages of electrochemical materials, such as extensive processing or fabrication techniques or a lack of sensing performance under practical conditions (i.e., humidity). Therefore, it is of great importance to create a sensor material that can

assist a sensor device to remain compact, practical, low-cost, and offer selective and real-time response at low operating temperatures. Furthermore, it is paramount to fabricate a surface chemistry that is solution processable, will meet the required sensing metrics relative to the state of the art, and does not require additional preparation processes or components to yield a response to formaldehyde.

Utilizing polymeric materials in sensing applications allows devices to remain compact with facile fabrication protocols while maintaining high performance. Polymer thin films composed of macromolecules such as poly(3-hexylthiophene) (P3HT), poly(ethyleneimine) (PEI), polypyrrole (PPy), and biodegradable polysaccharides have shown promise in the detection of formaldehyde [44-49]. Additionally, inks composed of these polymeric materials offer solution processability and require little to no additives to detect formaldehyde. Some of these sensors utilize microheaters and NiO thin films to detect formaldehyde at concentrations as low as 1.2 ppm [28], [50]. Yet, finding a non-chemiresistive sensor device platform that can utilize these polymer thin films while remaining at a small scale and low cost remains challenging. As such, there is much promise in combining polymers with resonant mass sensors. Resonant mass sensors, a form of gravimetric sensors, are inexpensive to manufacture, require low energy input to operate, and offer a robust sampling rate. In this effort, this is accomplished by utilizing an array of Pierce oscillators and a frequency counting algorithm that allows for the simultaneous monitoring of 16 sensors that have a temporal resolution of 1 s and frequency resolution of 1 Hz. This rapid and real-time detection approach yields a reliable sensor platform to monitor surface interactions with a target analyte. Recently, resonant mass sensors, when combined with a modified materials surface chemistry, have shown rapid and selective responses in the detection of aromatic VOC compounds [51]. Combining the robust, inexpensive, small-scale, and low-energy properties of a resonant mass sensor platform with the processable and chemically selective properties of polymer materials could enable the development of practical formaldehyde sensors for buildings.

Here, a resonant mass sensor was coated with poly (5-carboxyindole) (P5C). P5C has been used previously in electrochemical sensors for the detection of saturated ethanol, toluene, methanol, ether, and acetone vapors [52]. However, P5C has not been previously utilized for the detection of formaldehyde, and it has not been used to achieve lower gas detection limits (i.e., <100 ppm of analyte). Additionally, when 50% (by weight) of β-cyclodextrin (BCD) was blended with the P5C (P5C–BCD), the sensor showed improved performance. This improved performance agrees with previous literature where BCD has shown effective capture of formaldehyde and improved performance in air filtration systems [54-57]. Furthermore, by using the resonant mass sensor platform and this chemical functionalization protocol, formaldehyde was detected with rapid response and recovery times characterized by time constants of 27 s and 16 s, respectively. In comparison with other polymer-based sensing counterparts, this sensor offers straightforward implementation due to its high sensitivity, low operating temperature, and cyclability. Moreover, these sensors detect formaldehyde gas through physisorption, which allows for repeated use. The apparent adsorption of formaldehyde gas is related to the non-covalent interactions between P5C and formaldehyde. Importantly, this interaction can be enhanced using β-cyclodextrin. This surface chemistry allows for feasible solution processing and does not require any additional device manipulations to suffice sensing ability. Thus, this sensing material could offer an easily functionalized and cheap alternative capable of quick and reliable detection of formaldehyde gas.

Experimental methods

Materials

All of the chemicals utilized in this study were purchased from Sigma-Aldrich, and they were used as received unless otherwise noted. P5C was synthesized utilizing previously reported procedures [58]. The reaction was performed in a scintillation vial at room temperature (~25 °C). A 1:2 molar ratio of monomer to oxidizing agent was utilized for this polymerization. To begin the polymerization, 100 mg of 5-carboxyindole monomer (0.031 M) was dissolved in 1.5 mL of ethanol. To this monomer solution, a pre-prepared oxidizing agent solution of 0.062 M ammonium peroxodisulfate in 0.1 M H_2SO_4 (aq.) was added dropwise while maintaining constant stirring. As the reaction proceeded, a gradual darkening of the solution occurred, which indicated that the polymerization reaction had occurred. The resulting solution was left to continuously stir overnight. After stirring, the black precipitate solids were collected by centrifugation followed by washing with excess ethanol and water. The remaining polymer solids were then dried under vacuum (i.e., <1 Torr). P5C inks were prepared by dispersing P5C in an ethanol solution at a loading of 1.0 mg mL^{-1}. The P5C–BCD ink preparation followed the same protocol as P5C. However, in the P5C–BCD synthesis, prior to adding the ammonium peroxodisulfate in the 0.1 M H_2SO_4 solution, β-cyclodextrin was added in a 1:2 mass ratio relative to the 5-carboxindole monomer.

General methods

A Hitachi S-4800 Field Emission scanning electron microscope (SEM) was utilized to image the P5C and P5C–BCD polymer films. For each of these images, 1 µL of the P5C or P5C–BCD at a concentration of 1.0 mg mL^{-1} polymer solution was printed on a silicon dioxide substrate and dried under vacuum overnight. The films were then coated with 20 nm of carbon prior to imaging using a SPI carbon sputter coater to prevent charging during image acquisition. Attenuated total internal reflectance-Fourier transform infrared (ATR-FTIR) spectroscopy was performed using dried samples. The samples were placed on a diamond substrate of a Thermo-Nicolet Nexus FTIR using a deuterated triglycine sulfate KBr detector with a KBr beam splitter. Under a dry nitrogen purge, 100 scans were acquired over a range of 800 $cm^{-1} \leq \nu \leq 4500\ cm^{-1}$ for each sample. A TA SDT Q600 instrument was used for thermal gravimetric analysis of the samples. The samples were loaded into an alumina ceramic crucible and kept under ambient conditions, and then, they were heated from room temperature, at a rate of 10 °C min^{-1}, to a final temperature of 800 °C. A TA Instruments Q20 Series differential scanning calorimeter (DSC) was used for thermal transition analysis. The samples were sealed in Tzero hermetic pans, then annealed at 220 °C under a nitrogen gas purge, and then cooled to −50 °C, before the trace that started at −50 °C and ended at 220 °C (at a scan rate of 10 °C min^{-1}) was collected. A Kratos Axis Ultra DLD imaging X-ray photoelectron spectrometer with a monochromatic Al Kα (E = 1486.6 eV) was utilized for X-ray photoelectron spectroscopy (XPS) measurements, and these data were acquired while the sample was under high vacuum ($P \sim 10^{-9}$ Torr). CasaXPS software was utilized for all of the XPS data analyses.

Device functionalization

In the following experiments, small-scale quartz crystal resonators were functionalized by casting 1 µL of a 1 mg mL^{-1} solution of P5C or P5C–BCD onto the resonator surface. The devices were left to dry for at least 30 min under vacuum ($P \leq 0.4$ Torr) to remove any residual solvent.

Device instrumentation

The device instrumentation utilized in this work was previously reported [48]. An array of Pierce oscillators was used to evaluate the response of the devices to target analytes. Each oscillator consisted of a quartz crystal resonator (Kyocera Corp., CX3225) that had a capacitance of *CL* = 12 pF, an isolation resistor (R_2 = 510 Ω), one feedback resistor (R_1 = 2 MΩ), two load capacitors (C_1 = 22 pF and C_2 = 22 pF), and an inverter. The Pierce oscillator inverter and three additional inverters were provided by a crystal oscillator driver in order to convert the output signal to a square wave. These oscillators were then assembled as an array of 16 devices (Supplementary Information Figure S1a). To track oscillation frequency, a Field Programmable Gate Array (FPGA) was used as a frequency counter, which was also able to track all of the oscillators in parallel. With all of these components, a frequency resolution of 1 Hz was achieved for all 16 devices. For testing purposes, the 16 resonators were decoupled from the rest of the circuit but still connected to an instrumentation board. The instrumentation board contained the remaining elements of the circuit mentioned previously. By decoupling the circuit, functionalized resonators could be added and removed more efficiently.

Device testing

The testing protocols utilized in this work were reported previously [48]. The experimental setup shown in Supplementary Information Figure S1b was used to test the devices. A board with 16 resonators was first secured to an instrumentation board that was attached to the inside of a 9.5-cm-diameter chamber. The chamber remained at room temperature (~22.5 °C) and was sealed during testing. An in-line flow distribution system, which was connected to the chamber, controlled the concentrations of the target analytes. To control the concentration of analytes, air or nitrogen was passed through a series of mass flow controllers (MFC) in parallel. One MFC (MKS 1179A, 500 $cm^3\ min^{-1}$) led directly into the chamber while the other set of MFCs (MKS 1480A, 40 $cm^3\ min^{-1}$) passed through a bubbler (Chemglass, AF-0085), which contained 10 mL of the target analyte. These lines reconnected at a manifold and flowed into the chamber. Before and after the target analyte was introduced into the chamber, nitrogen or air was used to flush the chamber at a flow rate of 500 $cm^3\ min^{-1}$ so that the environment could remain inert. During experimentation, the frequency of each device was recorded using the FPGA and LabVIEW. To ensure the most accurate results, multiple similarly manufactured sensors were used for the same test. The responses from each of these sensors were averaged and reported as the representative response from our sensor. It should be noted that some figures below show the response from a single sensor, which may not exactly match the reported average response.

Results and discussion

Materials characterization

Upon drop casting and drying of the polymer films, a surface morphology unique to each film was observed under SEM imaging (Figure 1). When drop cast, P5C formed spherical sub-micron sized particles with some particles showing nanoscale features when they were not agglomerated (Figure 1a). The individual P5C nanoparticles had a spherical morphology. This spherical morphology is consistent with the polyindole class of polymers [59]. However, these particles were also observed to be agglomerated in patches as large as 5 µm in diameter (Figure 1a). Additionally, these 5 µm patches of agglomerated particles did not reside uniformly across the surface.

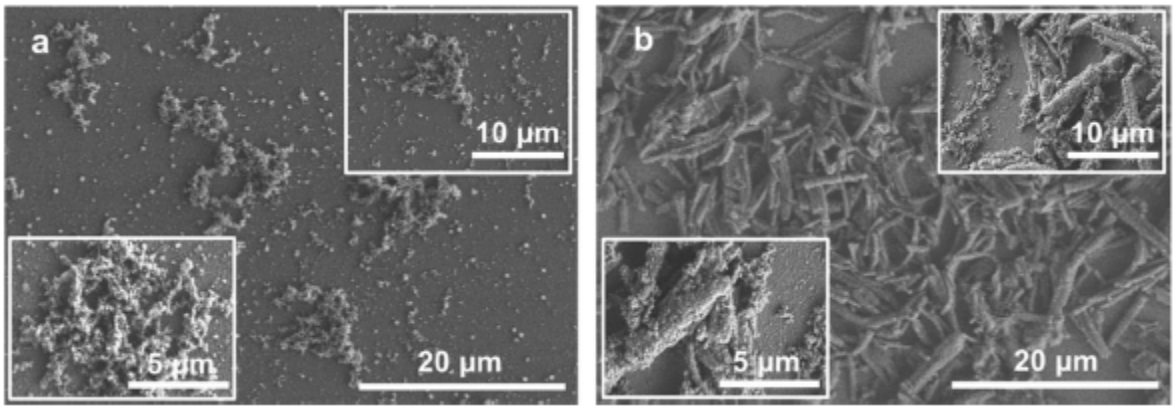

Figure 1. SEM images of a the P5C polymer and b P5C–BCD polymer after being dissolved in ethanol (1 mg mL−1), drop cast onto a silicon wafer, dried for 12 h under vacuum, and coated with carbon. The panels show the same films at three different magnification levels

On the other hand, when P5C–BCD was drop cast, it formed agglomerated micron-sized patches that uniformly coated the surface (Figure 1b). However, the individual particles that constituted these micron-sized patches had a cylindrical or tubular surface morphology. This cylindrical surface morphology, which was uniformly coated over the surface substrate, allowed for an increased lateral surface area of the surface chemistry. Thus, we believe that the combination of these features (i.e., better surface coating and larger surface area) in the P5C–BCD composites allowed for better interactions with formaldehyde gas because more of the surface chemistry contacted formaldehyde as it was present (vide infra).

The P5C–BCD composite structure expressed features of both P5C and BCD, as confirmed via FTIR spectroscopy (Figure 2a). As previously reported, the vibrational peaks of P5C include sharp C=O stretching (1690 cm^{-1}), sharp N–H bending (1534 cm^{-1}), sharp C=C alkene stretching (1450 cm^{-1}), sharp C–N aromatic stretching (1220 cm^{-1}), and sharp C–H bending 760 cm^{-1} spectra peaks [60]. These peaks are associated with the carboxylic acid, amine, and aromatic conjugated structural features of P5C (Figure 2b). Having these chemical functionalities is important as carboxylic acid functionalities have been shown to non-covalently interact with formaldehyde in related polymeric material [45]. BCD expressed broad O–H stretching at 3250 cm^{-1} and sharp C–O–C stretching (1077 cm^{-1}) spectral signals, which were in agreement with previous BCD studies [61]. The lack of chemical shifts of the P5C–BCD composite relative to the pristine P5C and BCD materials suggests that no chemical bonds were formed between BCD and P5C during the composite formulation, consistent with our expectations. Rather the functional groups for P5C and BCD remained intact and coexist in the composite material. Overall, this characterization shows the synthesis of P5C–BCD with the proper chemical functionalities to potentially interact with formaldehyde.

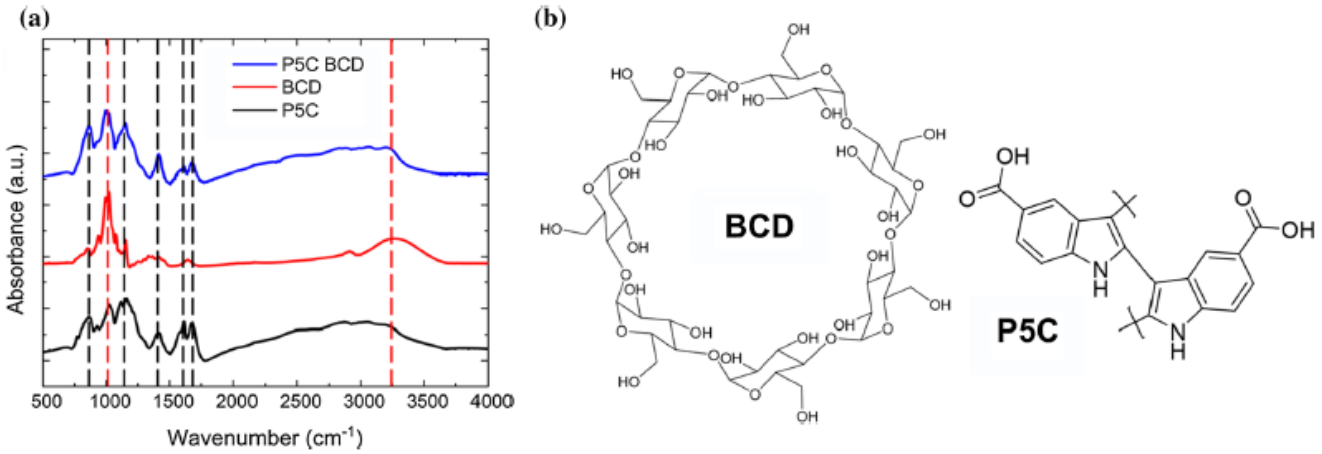

Figure 2. a Attenuated total internal reflectance-Fourier transform infrared (ATR-FTIR) spectra of the P5C, P5C–BCD, and BCD samples. These spectra highlight the sharp P5C peaks at 1690 cm−1, 1534 cm−1, 1450 cm−1, 1220 cm−1, and 760 cm−1 and broad (3250 cm−1) and sharp (1077 cm−1) BCD peaks, which appeared in the P5C–BCD nanocomposite. b Chemical structures of BCD (left) and P5C (right)

Upon heating, P5C–BCD expressed a higher melting point (*Tm* = 211 °C) relative to P5C (*Tm* = 199 °C), as shown in Figure 3a. This increase in *Tm* is likely due to the strong intermolecular forces between the BCD and P5C. Additionally, P5C–BCD showed a glass transition temperature (*Tg*) of 154 °C while P5C showed a *Tg* of 156 °C. Moreover, P5C degraded (i.e., passing 10% weight loss) after 225 °C while P5C–BCD showed degradation (i.e., passing 10% weight loss) after 300 °C (Figure 3b). The initial approximate 10% in weight loss in P5C and P5C–BCD and 14% weight loss in BCD is attributed to the loss of water entrained within the materials. BCD then showed a degradation (i.e., passing 14% weight loss) at 310 °C, which is characteristic of previous BCD TGA studies [61].

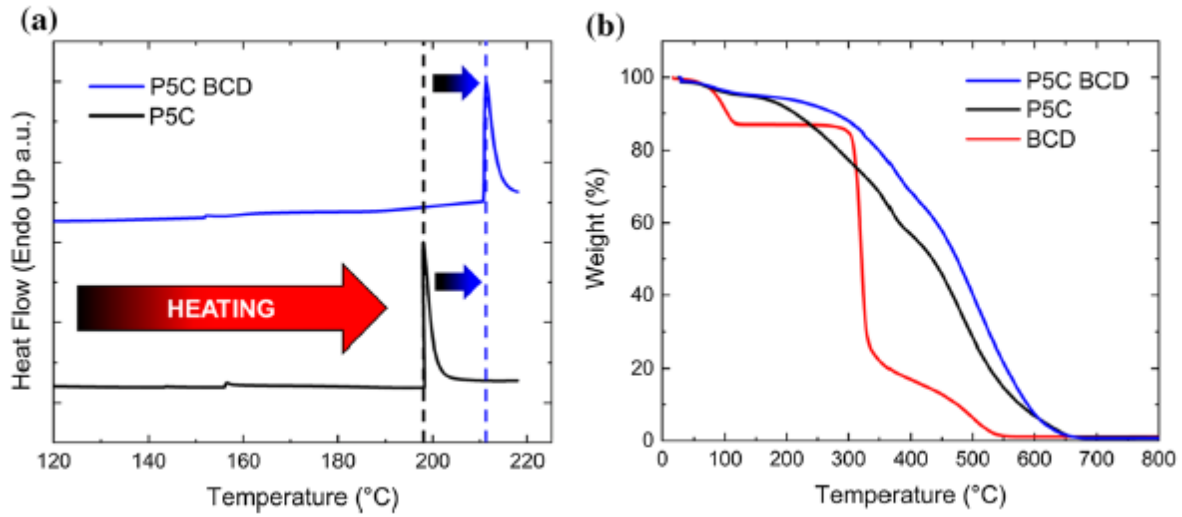

Figure 3. a DSC heating trace of P5C and P5C–BCD highlighting that P5C has approximately a Tg of 156 °C and a Tm of 199 °C while P5C-BCD has approximately a Tg of 154 °C and a Tm of 211 °C. Note, P5C–BCD showed a 12 °C increase in melting point. b Thermogravimetric analysis (TGA) of P5C, P5C–BCD, and BCD under ambient air conditions. This TGA study highlights P5C degradation (i.e., passing 10% weight loss) after 225 °C, P5C–BCD degradation (i.e., passing 10% weight loss) after 300 °C, and BCD degradation (i.e., passing 14% weight loss) at 310 °Cf

The improved thermal stability of the P5C–BCD composites is attributed to the following possible points. First, BCD has a higher degradation temperature, and adding BCD to the P5C increased the degradation temperature of the composite material. Because P5C–BCD has a higher loading of BCD, this then expressed more degradation characteristics of the BCD instead of the P5C. Second, BCD reduced the mobility of the P5C polymer chains due to the presence of strong intermolecular forces or partial non-covalent inclusion complexes between the BCD and P5C, and this in turn, caused increased thermal stability [62]. This reduction in mobility is common in systems where nanoparticles are added to a polymer [63]. Essentially, the thermal degradation of polymers starts with free radical formations at weak bonds or at chain ends, followed by their transfer to adjacent chains via interchain reactions [63]. However, when BCD is present, it suppressed the free radical transfer of the interchain reactions upon thermal ionization and as a result suppressed the degradation temperature and rate. Overall, these thermal characterization studies show that the P5C–BCD composite did not go through any thermal transitions, and it did not degrade anywhere near room temperature. These thermal properties are reassuring that this material can be utilized in an interior environment, where temperature might fluctuate (i.e., 20–30 °C), and maintain temperature stability as chemical recognition layer on a sensor.

The C 1s, N 1s, and O 1s binding energy regions were observed in the XPS spectra of both P5C and P5C–BCD upon the initial survey scans (Figure 4a). Focusing on the C 1s region (Figure 4b) for both P5C and P5C–-BCD, there was primarily a sp^2 C=C peak observed at 284.8 eV, which is associated with the conjugated aromatic structure of P5C. P5C also showed a peak at 285.8 eV, which was a characteristic peak of the C–N bond, resultant from the nitrogen heteroatom in the conjugated indole ring [65]. P5C–BCD did not show any C–N character, likely due to the low intensity of the peak, as there is a low concentration of nitrogen in the material once BCD is added. However, P5C–BCD did show a peak at 286.6 eV, which is in good agreement with C–O binding energy characteristics [66]. This C–O peak is due to the C–O binding that occurs on BCD as it is a cyclic oligosaccharide consisting of seven glucose units that all contain C–O bonds.

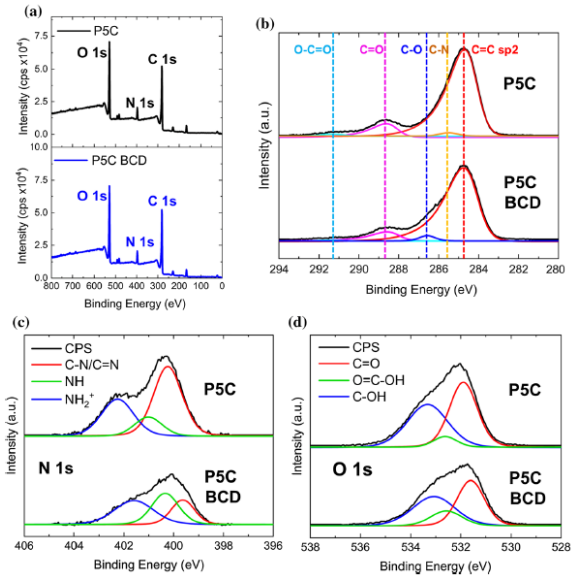

Figure 4. X-ray photoelectron spectroscopy analysis of P5C and P5C-BCD samples. a XPS survey spectra highlighting C 1s, N 1s, and O 1s in both the P5C and P5C–BCD samples. b P5C and P5C–BCD C 1s region of the

XPS spectra. Dashed lines in this region are highlighting carbon sp2, C–N, C–O, C = O, and O = C–O regions in the XPS spectra. c P5C and P5C–BCD N 1s region of the XPS spectra. This region is highlighting the different protonation states of the nitrogen in the P5C polymer. d P5C and P5C–BCD O 1s region of the XPS spectra. This region is highlighting the carboxylic acid groups in P5C as well as the C–OH character increase in P5C–BCD

There was no observation of C–O binding character in P5C alone; again, this is likely due to the low concentration of this type of bond. P5C and P5C–BCD did show a C=O binding energy at 288.6 eV and a small O–C=O binding energy at 291.1 eV due to the carboxylic acid functional group in the P5C structure [66]. Focusing on the N 1s region (Figure 4c), there were 3 characteristic binding peaks shown for P5C and P5C–BCD which correspond to the C–N/C=N, NH, and NH_2^+ bonds. C–N/C=N is expressed prevalently in both samples due to the nitrogen being in a conjugated indole structure in which carbon–nitrogen bonds can exist in a mixture of single and double bonded states. Importantly, P5C and P5C–BCD also showed varying levels of NH and NH_2^+ bonds in their N 1s regions as well. There have been previous XPS studies on conjugated polymers containing nitrogen which show that nitrogen binding energies can change based on their relative protonation state [67]. In P5C, there was a higher amount of nitrogen atoms in a more protonated state compared to the P5C–BCD samples (NH_2^+ >NH bonds). In P5C, upon synthesis in solution, the solution remained under low pH conditions due to the carboxylic acid groups present in the system. This prompted the nucleophilic nitrogen to enter proton exchange mechanisms with the carboxylic acid groups, and thus, the nitrogen existed in a more protonated state (Scheme 1). This indicates that there is also more unprotonated carboxylic acid groups present in the P5C as well. However, in P5C–BCD there is a greater amount of NH bonding character expressed in comparison with the NH_2^+, which is due to the pendant alcohol moieties on the BCD neutralized the unstable NH_2^+ and drove the proton exchange equilibrium to favor the neutral carboxylic acid and amine structure during synthesis in solution (NH). This is likely critical in terms of formaldehyde sensing as carboxylic acid groups can hydrogen bond more effectively with formaldehyde than their unprotonated carboxylate (COO^-) counterparts. Focusing on the O 1s binding region (Figure 4d), there was observed C=O, O–C–OH, and C–OH character which is expressed in both P5C and BCD due to the carboxylic acid and alcohol groups in P5C and BCD. BCD, due to the high concentration of pendant alcohols in its structure, created a high intensity of C–OH binding region which masks the majority of the carboxylic acid region. This, in turn, did not allow for relative comparison of carboxylic acid groups between the P5C and P5C–BCD, but rather just showed the appearance of both groups. Overall, P5C was observed to have indole features with carboxylic acid functional group which can alter protonation states based on the appearance or disappearance of BCD.

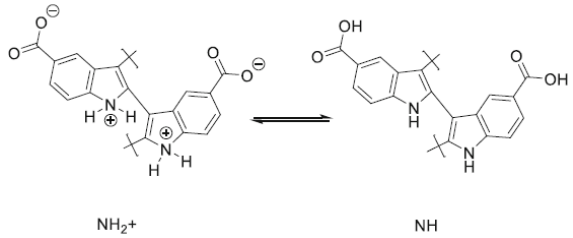

Scheme 1. Structure of P5C highlighting the proton exchange mechanism of P5C. Nitrogen protonation and carboxylic acid deprotonation showing the existence of NH and NH2+ states

Sensor performance

In a background of nitrogen, resonators functionalized with P5C and P5C–BCD produced oscillation frequency shifts when exposed to formaldehyde at various concentrations ranging from 25 to 100 ppm. To begin testing, a board of resonators was functionalized with 1 µL of a 1 mg mL^{-1} P5C solution or 1 µL of a 1 mg mL^{-1} P5C–BCD solution (i.e., each resonator was functionalized with only one type of chemistry, either P5C or P5C–BCD). After evaporation of the residual solvent, approximately 1 µg of functionalization chemistry remained on each resonator. The board was placed in the test chamber and the oscillation frequency of each resonator was recorded over time. Formaldehyde was introduced into the chamber in 20 min intervals at concentrations of 25, 50, and 100 ppm with a background of nitrogen. Twenty-minute intervals of nitrogen were used to purge the chamber between intervals of formaldehyde.

The concentration of formaldehyde was directly proportional to the frequency shifts from the oscillator board (Figure S2a). This test confirmed the detection of the formaldehyde gas at a concentration as low as 25 ppm in a background of nitrogen. Moreover, P5C–BCD yielded larger frequency shifts when exposed to formaldehyde under nitrogen background conditions relative to P5C (Figure 5a). When evaluated at concentrations lower than 25 ppm, P5C and P5C–BCD produced negligible frequency shifts compared to those observed from reference channels. The average sensitivity for the sensor in this environment was 13.7 ppm Hz^{-1} and 4.3 ppm Hz^{-1} for P5C and P5C–BCD, respectively. Frequency shifts from the reference channels can be attributed to small fluctuations in temperature and humidity within the testing chamber. This enhanced performance agreed with previous work, suggesting that cyclodextrin-based materials enhanced the uptake of formaldehyde

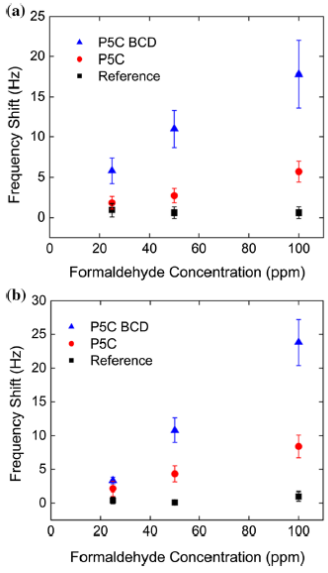

Figure 5. The average oscillation frequency shifts after 20 min plotted against different formaldehyde concentrations as recovered in a a background of nitrogen and b a background of air. Error bars represent one standard deviation from the average. Reference refers to an unfunctionalized device (no surface chemistry)

The functionalized resonators also produced significant oscillation frequency shifts when exposed to formaldehyde in a background of air (Figure S2b). Additionally, the average frequency shifts were approximately the same as the responses yielded from the test with a background gas of nitrogen

(Figure 5b). A linear relationship between oscillation frequency and formaldehyde concentration was found even when the background gas was changed from nitrogen to air. The average sensitivity for the sensor in this environment was 11.9 ppm Hz^{-1} and 7.7 ppm Hz^{-1} for P5C and P5C–BCD, respectively. Again, in this case, P5C-functionalized devices demonstrated less of a response with an air background relative to P5C–BCD functionalized sensors. It has been noted that residual moisture, temperature, or interfering gases being present in an air background can alter the adsorption properties of β-cyclodextrin [74]. Thus, we believe that the better performance of P5C–BCD over P5C in this case was caused by one of these variables.

To test the practicality of the materials chemistry, the sensors were tested in the presence of interfering analytes. The sensors functionalized with P5C or P5C–BCD detected formaldehyde in the presence of xylene, acetone, and methanol, which were introduced intentionally to serve as interfering gases. Each interfering analyte was added into the chamber at 500 ppm and 1000 ppm for 20 min intervals with a background of nitrogen. For comparison, formaldehyde at 1000 ppm was tested separately (Supplementary Information Figure S3). When each analyte was tested separately without any formaldehyde present, most of the interfering analytes showed minimal response (Figure 6a). Xylene at a concentration of 1000 ppm was the only analyte to generate a significant response from our surface chemistry without formaldehyde present. This is likely because xylene condensed on the surface over time due to its relatively low vapor pressure, which caused the observed response at higher gas concentrations. Moreover, as depicted in Figure 6b, the sensors produced significant oscillation frequency shifts in response to formaldehyde when interfering gases were present with the formaldehyde. These responses to formaldehyde were significant with both the P5C and P5C–BCD functional chemistries. As shown in Table 1a, the average frequency shift for resonators exposed to formaldehyde at all of the concentrations was 11.2 Hz, while the interfering gases had a maximum frequency shift of 5.9 Hz from xylene at 1000 ppm after accounting for frequency shifts from reference channels. While resonators functionalized with P5C and P5C–BCD produced frequency shifts when exposed to xylene, these shifts were markedly smaller than the frequency shifts relative to when exposed to formaldehyde alone. Additionally, almost no response was observed when the resonators were exposed to acetone or methanol (Table 1). However, there was an observed frequency shift having an average magnitude of 7.1 Hz larger when formaldehyde is present, indicating that formaldehyde could still be detected in the presence of other interfering analytes. Thus, formaldehyde could effectively be detected with these materials in the presence of interfering gases that could exist in interior locations.

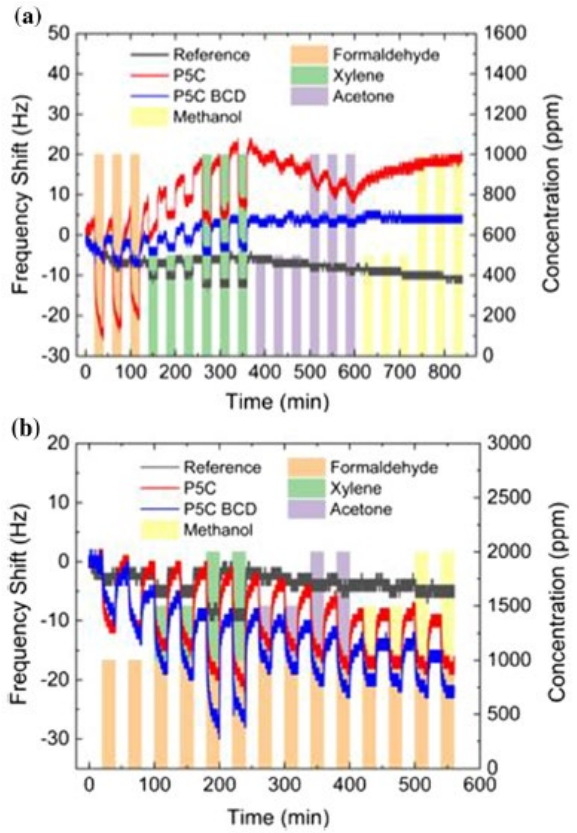

Figure 6. a Resonators exposed to 20 min pulses of formaldehyde, methanol, acetone, and xylene separately at concentrations of 500 ppm and 1000 ppm with a background of nitrogen. b Resonators exposed to 20 min pulses of methanol, acetone, and xylene at concentrations of 500 and 1000 ppm in the presence of 1000 ppm formaldehyde with a background of nitrogen. Reference refers to an unfunctionalized device (no surface chemistry)

Table 1. The average frequency shift of resonators functionalized with 1 µL of P5C solution, 1 µL of P5C–BCD solution, or left unfunctionalized (i.e., reference)

Analyte concentration	**Functionalization chemistry without exposure to formaldehyde**			**Functionalization chemistry with exposure to formaldehyde at 1000 ppm**		
	Reference	**P5C**	**P5C–BCD**	**Reference**	**P5C**	**P5C–BCD**
Xylene 500 ppm	2.7 Hz	3.9 Hz	2.6 Hz	3.3 Hz	12.3 Hz	14.0 Hz
Xylene 1000 ppm	5.4 Hz	11.3 Hz	6.1 Hz	7.1 Hz	17.0 Hz	17.7 Hz
Acetone 500 ppm	0.9 Hz	1.4 Hz	1.1 Hz	1.8 Hz	6.6 Hz	11.3 Hz
Acetone 1000 ppm	0.7 Hz	3.9 Hz	1.2 Hz	1.0 Hz	7.8 Hz	11.3 Hz
Methanol 500 ppm	0.6 Hz	0.8 Hz	0.2 Hz	0.9 Hz	5.6 Hz	8.5 Hz
Methanol 1000 ppm	0.7 Hz	1.1 Hz	0.2 Hz	1.1 Hz	5.9 Hz	9.5 Hz

Resonators were exposed to 20 min pulse of xylene, acetone, and methanol. The resonators were then run again in similar conditions, except that the resonators were tested in the presence of formaldehyde at 1000 ppm in each 20 min pulse at the same time as the other analytes.

While the relative humidity of the testing environment altered the response of the sensor, significant oscillation frequency shifts were still generated in response to formaldehyde. To understand the effect of humidity on device sensitivity, a board with resonators functionalized with either P5C or P5C–BCD was placed in a chamber with varying humidity levels (Figure 7). The relative humidity in the chamber ranged from 0 to 80% in increments of 20%, while formaldehyde was introduced in 30 min intervals. After formaldehyde, pure nitrogen was introduced in 30 min intervals between formaldehyde pulses to purge the chamber of formaldehyde. When conducting these experiments, the functionalized resonators provided responses to formaldehyde up to 80% relative humidity. There was an increase in frequency shift as the relative humidity was increased, and this is likely due to the hydrophilic nature of the P5C and P5C–BCD (Figure 8). However, as the testing continued, there was an overall downward drift in oscillation frequency as shown clearly in Figure 7d, e. We speculate that this downward drift (Figure7) was due to the accumulation of moisture on the surface of the resonator. This test indicates that formaldehyde can be detected at different levels of relative humidity with two different chemistries up to 60% relative humidity levels. Resonators functionalized with P5C–BCD had greater overall frequency responses during the duration of the test even at higher relative humidity levels.

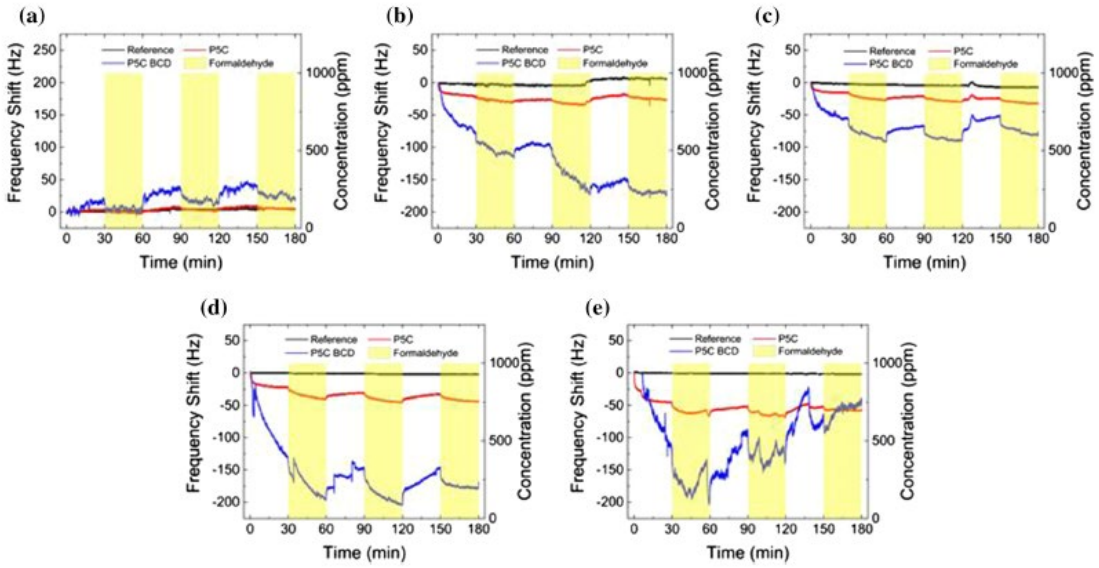

Figure 7. Resonators were exposed to 30 min pulse of formaldehyde at concentrations of 1,000 ppm with a background of nitrogen and different relative levels of humidity: a 0% relative humidity, b 20% relative humidity, c 40% relative humidity, d 60% relative humidity, and e 80% relative humidity. Relative humidity values were measured at a dry bulb temperature of 22.5 °C. The red and blue lines refer to the oscillation frequency shift with respect to time of resonators functionalized with 1 µL of P5C solution and 1 µL of P5C–BCD solution, respectively. The black lines represent the oscillation frequency shift of an unfunctionalized resonator (i.e., reference). Yellow bars indicate the presence of formaldehyde

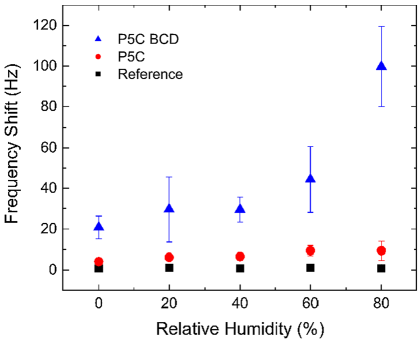

Figure 8. The average oscillation frequency shift of resonators functionalized with 1 µL of P5C solution or 1 µL of P5C–BCD solution with respect to each relative humidity level. Resonators were exposed to 30 min pulses of formaldehyde at 1000 ppm at different levels of relative humidity. Error bars represent one standard deviation from the average. Reference refers to an unfunctionalized device (no surface chemistry)

As the relative humidity levels increased, the P5C–BCD produced greater responses to formaldehyde for a variety of reasons. First, formaldehyde could be better adsorbed into the BCD hydrophobic cavity. Due to the hydrophobic cavity and hydrophilic exterior of the β-cyclodextrin, this creates an ideal host–guest interaction with formaldehyde, even as the relative humidity levels increase. On the other hand, when β-cyclodextrin was present at lower relative humidity levels, there were also better responses to formaldehyde. Thus, we also put forward that β-cyclodextrin can not only act as a robust host for formaldehyde, but it can also act as a spacer in the P5C. It was observed upon the drop casting and drying of the polymer films that there was a surface texture unique to each film. When drop cast, P5C forms a more uniform film with spherical morphologies (Figure 1). However, when P5C–BCD is cast, it forms a more rigid textured and disrupted surface with cylindrical or tubular morphologies (Figure 1). At lower relative humidity levels, the P5C–BCD, due to the formed cylindrical rigid surface, allowed for more lateral surface area. This, in turn, allowed better diffusion of formaldehyde gas into the material and allowed formaldehyde to better interact with the surface chemistry. In this case, the host–guest interactions in the P5C–BCD thin films are not utilized because there is a low abundance of water. In turn, more surface interactions are a product of better diffusion of the gas into the material. Third, BCD allows for more carboxylic acid groups to remain protonated on the P5C polymer chain. As shown in the XPS N 1s region (Figure 4c), in P5C–BCD there was a higher amount of NH bonds over NH_2^+ bonds present in the sample in comparison with P5C. Due to the pendant alcohol moieties in the BCD, this, in turn, buffers the system, allowing for the proton exchange equilibrium to favor the NH state (Scheme 1). The NH state allows for a higher amount of carboxylic acid groups to be present which can hydrogen bond more effectively with formaldehyde and thus produce greater sensors responses. We believe the synergy of these three plausible sensing mechanisms allows for a robust formaldehyde sensing chemistry capable of detecting formaldehyde down to 25 ppm concentration levels in a variety of practical indoor environments.

Conclusions

A resonant mass sensor coated with P5C or P5C–BCD was utilized for enhanced formaldehyde sensing. P5C enabled enhanced adsorption of formaldehyde on the resonant mass sensor to 25 ppm levels. Moreover, the response of P5C to formaldehyde can be further enhanced by blending P5C with BCD, which allows for better diffusion of formaldehyde gas into the material, a hydrophobic cavity suitable for capturing formaldehyde, and more carboxylic acid moieties to promote better formaldehyde

adsorption in a humid environment. This work implemented a feasible chemical treatment protocol combined with the practical utilization of resonant mass sensors to create a robust sensing platform suitable for the detection of formaldehyde. We anticipate that these materials will be utilized further in future formaldehyde sensing studies to reach lower concentration detection limits while leveraging the materials properties of P5C and BCD in a useful manner. Overall, this formaldehyde sensor materials chemistry offers an inexpensive, facile to synthesize, and processable material which makes it a practical commercial contender for the interior monitoring of formaldehyde.

Acknowledgements

This work was funded by the Center for High Performance Buildings at Purdue University (Grant Number: CHPB-44-2019).

Supplementary Information

Below is the link to the electronic supplementary material.

Graph: Supplementary file1 (PDF 527 KB)

Publisher's Note

References

Chung PR, Tzeng CT, Ke MT, Lee CY. Formaldehyde gas sensors: a review. Sens (Switzerl). 2013; 13: 4468-4484. 1:CAS:528:DC%2BC3sXmtFWksLs%3D

Castro-Hurtado I, Mandayo GG, Castaño E. Conductometric formaldehyde gas sensors. A review: from conventional films to nanostructured materials. Thin Solid Films. 2013; 548: 665-676. 1:CAS:528:DC%2BC3sXotlOkurc%3D

Flueckiger J, Ko FK, Cheung KC. Microfabricated formaldehyde gas sensors. Sensors. 2009; 9: 9196-9215. 1:CAS:528:DC%2BD1MXhsVylurvJ

Chan WH, Xie TY. Determination of sub-ppbv levels of formaldehyde in ambient air using Girard's reagent T-coated glass fiber filters and adsorption voltammetry. Anal Chim Acta. 1997; 349: 349-357. 1:CAS:528:DyaK2sXlsFaiurw%3D

Meyer B, Andrews BAK, Reinhardt RM. Formaldehyde release from wood products. Anal Chem. 1986; 58: 1364

Cincinelli A, Martellini T. Indoor air quality and health. Int J Environ Res Public Health. 2017; 14: 1286

Kawamura K, Kerman K, Fujihara M. Development of a novel hand-held formaldehyde gas sensor for the rapid detection of sick building syndrome. Sens Actuat B Chem. 2005; 105: 495-501. 1:CAS:528:DC%2BD2MXit1anu7o%3D

Sekine Y, Nishimura A. Removal of formaldehyde from indoor air by passive type air-cleaning materials. Atmos Environ. 2001; 35: 2001-2007. 1:CAS:528:DC%2BD3MXhslOgsL0%3D

Hu J, Wu X, Zeng W. Formaldehyde sensor based on polypyrrole/β-cyclodextrin. J Control Release. 2011; 152: e211-e213. 1:CAS:528:DC%2BC3MXhs1KqtrzJ

Partanen T, Kauppinen T, Hernberg S. Formaldehyde exposure and respiratory cancer among woodworkers: an update. Scand J Work Environ Health. 1990; 16: 394-400. 1:CAS:528:DyaK3MXisFehs7c%3D

Gupta KC, Ulsamer AG, Preuss PW. Formaldehyde in indoor air: sources and toxicity. Environ Int. 1982; 8: 349-358. 1:CAS:528:DyaL3sXnslejtw%3D%3D
Kim WJ, Terada N, Nomura T. Effect of formaldehyde on the expression of adhesion molecules in nasal microvascular endothelial cells: the role of formaldehyde in the pathogenesis of sick building syndrome. Clin Exp Allergy. 2002; 32: 287-295. 1:CAS:528:DC%2BD38Xis1ektbw%3D
Hauptmann M. Mortality from lymphohematopoietic malignancies among workers in formaldehyde industries. Cancer Spect Knowl Environ. 2003; 95: 1615-1623. 1:CAS:528:DC%2BD3sXptVequrc%3D
Pinkerton LE, Hein MJ, Stayner LT. Mortality among a cohort of garment workers exposed to formaldehyde: an update. Occup Environ Med. 2004; 61: 193-200. 1:STN:280:DC%2BD2c%2FpsF2ktQ%3D%3D
Zhang L, Steinmaus C, Eastmond DA. Formaldehyde exposure and leukemia: a new meta-analysis and potential mechanisms. Mutat Res Mutat Res. 2009; 681: 150-168. 1:CAS:528:DC%2BD1MXhsFOlt7s%3D
Wang R, Zhang Y, Lan Q. Occupational exposure to solvents and risk of non-Hodgkin lymphoma in Connecticut women. Am J Epidemiol. 2009; 169: 176-185
Air Quality Guidelines, 2nd ed; WHO Regional Office for Europe: Copenhagen, Denmark, 2001. 15.
Occupational Safety and Health Guideline for Formaldehyde Potential Human Carcinogen; US Department of Health and Human Services: Washington, DC, USA, 1988. 16.
Chen D, Yuan YJ. Thin-film sensors for detection of formaldehyde: a review. IEEE Sens J. 2015; 15: 6749-6760. 1:CAS:528:DC%2BC28XhvFWmtLfL
Dojahn JG, Wentworth WE, Stearns SD. Characterization of formaldehyde by gas chromatography using multiple pulsed-discharge photoionization detectors and a flame ionization detector. J Chromatogr Sci. 2001; 39: 54-58. 1:CAS:528:DC%2BD3MXhtFeru7Y%3D
Davenport JJ, Hodgkinson J, Saffell JR, Tatam RP (2014) Formaldehyde sensor using non-dispersive UV spectroscopy at 340nm. 9141:91410K.
Septon JC, Ku JC. Workplace air sampling and polarographic determination of formaldehyde. Am Ind Hyg Assoc J. 1982; 43: 845-852. 1:CAS:528:DyaL38Xmt1WqtLo%3D
Möhlmann GR. Formaldehyde detection in air by laser-induced fluorescence. Appl Spectrosc. 1985; 39: 98-101
van den Broek J, Klein Cerrejon D, Pratsinis SE, Güntner AT. Selective formaldehyde detection at ppb in indoor air with a portable sensor. J Hazard Mater. 2020; 399: 123052
Tian H, Fan H, Li M, Ma L. Zeolitic imidazolate framework coated ZnO nanorods as molecular sieving to improve selectivity of formaldehyde gas sensor. ACS Sens. 2016; 1: 243-250. 1:CAS:528:DC%2BC2MXitVGrsrnI
Wang Z, Hou C, De Q. One-step synthesis of Co-doped In2O3 nanorods for high response of formaldehyde sensor at low temperature. ACS Sens. 2018; 3: 468-475. 1:CAS:528:DC%2BC1cXhtF2msrg%3D
Ishihara S, Labuta J, Nakanishi T. Amperometric detection of sub-ppm formaldehyde using single-walled carbon nanotubes and hydroxylamines: a referenced chemiresistive system. ACS Sens. 2017; 2: 1405-1409. 1:CAS:528:DC%2BC2sXhs1Gjtr%2FM
Wang YH, Lee CY, Lin CH, Fu LM. Enhanced sensing characteristics in MEMS-based formaldehyde gas sensors. Microsyst Technol. 2008; 14: 995-1000. 1:CAS:528:DC%2BD1cXmsVagsLo%3D
Asri MIA, Hasan MN, Fuaad MRA. MEMS gas sensors: a review. IEEE Sens J. 2021; 21: 18381-18397. 1:CAS:528:DC%2BB3MXitFygs7vO

Zhou Z-L, Kang T-F, Zhang Y, Cheng S-Y. Electrochemical sensor for formaldehyde based on Pt–Pd nanoparticles and a Nafion-modified glassy carbon electrode. Microchim Acta. 2009; 164: 133-138. 1:CAS:528:DC%2BD1MXlvFOksw%3D%3D

Chen T, Liu QJ, Zhou ZL, Wang YD. The fabrication and gas-sensing characteristics of the formaldehyde gas sensors with high sensitivity. Sens Actuat B Chem. 2008; 131: 301-305. 1:CAS:528:DC%2BD1cXktlOitrg%3D

Dirksen JA, Duval K, Ring TA. NiO thin-film formaldehyde gas sensor. Sens Actuat B Chem. 2001; 80: 106-115. 1:CAS:528:DC%2BD3MXosFyitrY%3D

Knake R, Jacquinot P, Hodgson AWE, Hauser PC. Amperometric sensing in the gas-phase. Anal Chim Acta. 2005; 549: 1-9. 1:CAS:528:DC%2BD2MXpt1WktLg%3D

Wang H, Chi Y, Gao X. Amperometric formaldehyde sensor based on a Pd nanocrystal modified C/Co2P electrode. J Chem. 2017; 2017: 2346895

McGinn CK, Lamport ZA, Kymissis I. Review of gravimetric sensing of volatile organic compounds. ACS Sens. 2020; 5: 1514-1534. 1:CAS:528:DC%2BB3cXptlGls7o%3D

Choi N-J, Lee H-K, Moon SE. Ultrafast response sensor to formaldehyde gas based on metal oxide. J Nanosci Nanotechnol. 2014; 14: 5807-5810. 1:CAS:528:DC%2BC2cXhvVCmu73K

Zhou W, Wu Y-P, Zhao J. Efficient gas-sensing for formaldehyde with 3D hierarchical Co3O4 derived from Co5-based MOF microcrystals. Inorg Chem. 2017; 56: 14111-14117. 1:CAS:528:DC%2BC2sXhslKqtLrI

Bouchikhi B, Chludziński T, Saidi T. Formaldehyde detection with chemical gas sensors based on WO3 nanowires decorated with metal nanoparticles under dark conditions and UV light irradiation. Sens Actuat B Chem. 2020; 320: 128331. 1:CAS:528:DC%2BB3cXhtVCru7jL

Zhang D, Liu J, Jiang C. Quantitative detection of formaldehyde and ammonia gas via metal oxide-modified graphene-based sensor array combining with neural network model. Sens Actuat B Chem. 2017; 240: 55-65. 1:CAS:528:DC%2BC28XhsVCmsrrO

Zaki M, Hashim U, Arshad MKM, et al (2016) Sensitivity and selectivity of metal oxides based sensor towards detection of formaldehyde. In: Proceedings of the 2016 IEEE international conference on semiconductor electronics (ICSE). pp 312–315

Diltemiz SE, Ecevit K (2019) High-performance formaldehyde adsorption on CuO/ZnO composite nanofiber coated QCM sensors. J Alloys Compd 783:608–616.

Hussain M, Kotova K, Lieberzeit PA. Molecularly imprinted polymer nanoparticles for formaldehyde sensing with QCM. Sensors. 2016; 16: 1011

Feng L, Feng L, Li Q. Sensitive formaldehyde detection with QCM sensor based on PAAm/MWCNTs and PVAm/MWCNTs. ACS Omega. 2021; 6: 14004-14014. 1:CAS:528:DC%2BB3MXhtFentL7E

Tai H, Jiang Y, Duan C. Development of a novel formaldehyde OTFT sensor based on P3HT/Fe2O3 nanocomposite thin film. Integr Ferroelectr. 2013; 144: 15-21. 1:CAS:528:DC%2BC3sXhtFemtbfO

Tang X, Raskin J-P, Lahem D. A Formaldehyde Sensor Based on Molecularly-Imprinted Polymer on a TiO2 nanotube array. Sensors (Basel). 2017; 17: 675

Rovina K, Vonnie JM, Shaeera SN. Development of biodegradable hybrid polymer film for detection of formaldehyde in seafood products. Sens Bio-Sens Res. 2020; 27: 100310

Zhang D, Zhang M, Ding F. Efficient removal of formaldehyde by polyethyleneimine modified activated carbon in a fixed bed. Environ Sci Pollut Res. 2020; 27: 18109-18116. 1:CAS:528:DC%2BB3cXlt1Smsbk%3D

Tai H, Bao X, He Y. Enhanced formaldehyde-sensing performances of mixed polyethyleneimine-multiwalled carbon nanotubes composite films on quartz crystal microbalance. IEEE Sens J. 2015; 15: 6904-6911. 1:CAS:528:DC%2BC28XhvFWmtLfJ

Ariyageadsakul P, Vchirawongkwin V, Kritayakornupong C. Role and impact of differently charged polypyrrole on formaldehyde sensing behavior. Synth Met. 2017; 230: 27-38. 1:CAS:528:DC%2BC2sXps1KgsrY%3D

Lee CY, Hsieh PR, Lin CH et al (2006) MEMS-based formaldehyde gas sensor integrated with a micro-hotplate. Microsystem Technologies. pp 893–898.

Hodul JN, Murray AK, Carneiro NF. Modifying the surface chemistry and nanostructure of carbon nanotubes facilitates the detection of aromatic hydrocarbon gases. ACS Appl Nano Mater. 2020; 3: 10389-10398. 1:CAS:528:DC%2BB3cXitVant73P

Bartlett PN, Ling-Chung SK. Conducting polymer gas sensors part III: results for four different polymers and five different vapours. Sens Actuat. 1989; 20: 287-292. 1:CAS:528:DyaK3MXhs1yntQ%3D%3D

Bartlett PN, Archer PBM, Ling-Chung SK. Conducting polymer gas sensors part I: fabrication and characterization. Sens Actuat. 1989; 19: 125-140. 1:CAS:528:DyaK3cXks1Wrs7g%3D

Noreña-Caro D, Álvarez-Láinez M. Functionalization of polyacrylonitrile nanofibers with β-cyclodextrin for the capture of formaldehyde. Mater Des. 2016; 95: 632-640

Wang L, Kang Y, Xing C-Y. β-Cyclodextrin based air filter for high-efficiency filtration of pollution sources. J Hazard Mater. 2019; 373: 197-203. 1:CAS:528:DC%2BC1MXlvVaju7c%3D

Kadam V, Truong YB, Schutz J. Gelatin/β–Cyclodextrin Bio-Nanofibers as respiratory filter media for filtration of aerosols and volatile organic compounds at low air resistance. J Hazard Mater. 2021; 403. 1:CAS:528:DC%2BB3cXhvVWjt77O

Kadam V, Truong YB, Easton C. Electrospun polyacrylonitrile/β-cyclodextrin composite membranes for simultaneous air filtration and adsorption of volatile organic compounds. ACS Appl Nano Mater. 2018; 1: 4268-4277. 1:CAS:528:DC%2BC1cXhtlWhsrjF

Joshi L, Gupta B, Prakash R. Chemical synthesis of poly(5-carboxyindole) and poly(5-carboxyindole)/carboxylated multiwall carbon nanotube nanocomposite. Thin Solid Films. 2010; 519: 218-222. 1:CAS:528:DC%2BC3cXht1Kgt7%2FO

Gupta B, Chauhan DS, Prakash R. Controlled morphology of conducting polymers: Formation of nanorods and microspheres of polyindole. Mater Chem Phys. 2010; 120: 625-630. 1:CAS:528:DC%2BC3cXivVygtLs%3D

Joshi L, Prakash R. Synthesis of conducting poly(5-carboxyindole)/Au nanocomposite: investigation of structural and nanoscale electrical properties. Thin Solid Films. 2013; 534: 120-125. 1:CAS:528:DC%2BC3sXktFahsLg%3D

Abarca RL, Rodríguez FJ, Guarda A. Characterization of beta-cyclodextrin inclusion complexes containing an essential oil component. Food Chem. 2016; 196: 968-975. 1:CAS:528:DC%2BC2MXhs1KktrrK

Wang X, Xing W, Wang B. Comparative study on the effect of beta-cyclodextrin and polypseudorotaxane As carbon sources on the thermal stability and flame retardance of polylactic acid. Ind Eng Chem Res. 2013; 52: 3287-3294. 1:CAS:528:DC%2BC3sXhs1Ojsrs%3D

Mbhele ZH, Salemane MG, van Sittert CGCE. Fabrication and characterization of silver−polyvinyl alcohol nanocomposites. Chem Mater. 2003; 15: 5019-5024. 1:CAS:528:DC%2BD3sXptlGqt74%3D

Afzal AB, Akhtar MJ, Nadeem M, Hassan MM. Investigation of structural and electrical properties of polyaniline/gold nanocomposites. J Phys Chem C. 2009; 113: 17560-17565. 1:CAS:528:DC%2BD1MXhtFWqu7rK

Yan X, Xu T, Chen G. Preparation and characterization of electrochemically deposited carbon nitride films on silicon substrate. J Phys D Appl Phys. 2004; 37: 907-913. 1:CAS:528:DC%2BD2cXivVynsLo%3D

Chen X, Wang X, Fang D. A review on C1s XPS-spectra for some kinds of carbon materials. Fuller Nanotub Carbon Nanostruct. 2020; 28: 1048-1058. 1:CAS:528:DC%2BB3cXhsVKksLnM

Neoh KG, Kang ET, Tan KL. Protonation and deprotonation behaviour of amine units in polyaniline. Polymer (Guildf). 1993; 34: 1630-1636. 1:CAS:528:DyaK3sXisFGmsr4%3D

Tong Z, Yang Y, Wang J. Layered polyaniline/graphene film from sandwich-structured polyaniline/graphene/polyaniline nanosheets for high-performance pseudosupercapacitors. J Mater Chem A. 2014; 2: 4642-4651. 1:CAS:528:DC%2BC2cXjsVKjtbY%3D

Wang L, Liang X-Y, Chang Z-Y. Effective formaldehyde capture by green cyclodextrin-based metal–organic framework. ACS Appl Mater Interf. 2018; 10: 42-46. 1:CAS:528:DC%2BC2sXhvFOitbbO

Yang Z, Miao H, Rui Z, Ji H. Enhanced formaldehyde removal from air using fully biodegradable chitosan grafted β-cyclodextrin adsorbent with weak chemical interaction. Polymers (Basel). 2019; 11: 276

Kadam V, Kyratzis IL, Truong YB. Air filter media functionalized with β-cyclodextrin for efficient adsorption of volatile organic compounds. J Appl Polym Sci. 2020; 137: 49228. 1:CAS:528:DC%2BB3cXkvF2gsL8%3D

Liu Z, Yan A, Miao R (2010) Removal of indoor pollutants by nano TiO2/beta-cyclodextrin coated paper under UV irradiation. In: Proceedings of the 2010 4th international conference on bioinformatics and biomedical engineering, pp 1–4.

Yu X, Qi H, Huang Z. Preparation and characterization of spherical β-cyclodextrin/urea–formaldehyde microcapsules modified by nano-titanium oxide. RSC Adv. 2017; 7: 7857-7863. 1:CAS:528:DC%2BC2sXhtlelsbw%3D

Zhao W, Shi B, Hu C. Adsorption properties of β-cyclodextrin for adsorbing aromatic hydrocarbons from the gas phase and water. J Macromol Sci B. 2007; 47: 211-216